frontiers | Frontiers in Earth Science

TYPE Original Research
PUBLISHED 06 September 2022
DOI 10.3389/feart.2022.927826

OPEN ACCESS

EDITED BY
Mélanie Davranche,
University of Rennes 1, France

REVIEWED BY
Jun Shen,
China University of Geosciences
Wuhan, China
Way Foong Lim,
Universiti Sains Malaysia (USM), Malaysia

*CORRESPONDENCE
Xiao-Ming Liu,
xiaomliu@unc.edu

SPECIALTY SECTION
This article was submitted to Geochemistry,
a section of the journal
Frontiers in Earth Science

RECEIVED 25 April 2022
ACCEPTED 18 July 2022
PUBLISHED 06 September 2022

CITATION
Cao C, Liu X-M and Chen J (2022), Cerium anomaly as a tracer for paleo-oceanic redox conditions: A thermodynamics-based Ce oxidation modeling approach.
Front. Earth Sci. 10:927826.
doi: 10.3389/feart.2022.927826

Cerium anomaly as a tracer for paleo-oceanic redox conditions: A thermodynamics-based Ce oxidation modeling approach

Cheng Cao[1,2], Xiao-Ming Liu[2]* and Jun Chen[1]

[1]MOE, Key Laboratory of Surficial Geochemistry, School of Geological Sciences and Engineering, Nanjing University, Nanjing, China, [2]Department of Earth, Marine, and Environmental Sciences, University of North Carolina at Chapel Hill, Chapel Hill, NC, United States

Reconstructing redox conditions in the paleo-ocean is essential to understand the Earth's biogeochemical evolution. Cerium (Ce) anomaly in marine sediments has been used to distinguish oxic versus anoxic depositional environments in the Paleo-ocean. Previous studies suggested that dissolved oxygen is indispensable to cerium oxidation. Therefore, this reaction can be thermodynamically modeled to quantify oxygen contents in the ocean. This study presents a series of thermodynamics-based models to relate Ce anomaly to dissolved oxygen level. We then evaluated these models in two representatively settings, including an oxic ocean and anoxic basin. Finally, we examined the modeled relationship on a compiled dataset of cerium anomaly and dissolved oceanic oxygen content. These models suggest that the cerium anomaly is quantitatively related to oceanic oxygen, pH, and phosphate concentration. Notably, the results suggest that cerium anomaly is not sensitive to changes in dissolved oxygen in oxic environments. By contrast, Ce anomaly is well correlated with dissolved oxygen in anoxic environments, and it was less affected by pH and phosphate concentration. This research has significant implications for using lanthanide patterns in ancient marine carbonates to quantify dissolved oxygen level, especially during anoxic events in the Paleo-ocean.

KEYWORDS

Ce anomaly, Paleo-ocean redox, thermodynamic modeling, rare earth elements, oxidation-reduction reactions

1 Introduction

The oxygen level of Earth surface plays a significant role in biosphere evolution (Canfield, 2005; Holland, 2006). Particularly, constraining oxygen levels in the ocean and atmosphere helps to determine the threshold for biological diversification and mass extinction events. However, proxy-based estimates of both atmospheric and oceanic oxygen could vary significantly among various geochemical tracers (Algeo and Tribovillard, 2009; Algeo and Li, 2020; Bellefroid et al., 2018; Canfield, 2005; Chen et al., 2021; Lyons et al., 2014; Liu et al., 2016; Lu et al., 2018; Livermore et al., 2020; Nielsen

et al., 2017; Ostrander et al., 2019; Planavsky et al., 2014; Wallace et al., 2017; Zhang et al., 1998). Therefore, reliable/refined proxies are still needed to provide robust reconstructions of oxygen through Earth history. Among various proxies, the cerium (Ce) anomaly in pristine marine sediments have been widely used to infer oxic versus anoxic depositional environments (Alibo and Nozaki, 1999; Behrens et al., 2018a; German et al., 1991; Kamber et al., 2014; Ling et al., 2013; Tostevin et al., 2016; Webb and Kamber, 2000; Zhang and Shields, 2022). Because rare Earth elements (REEs) incorporate into the calcite lattice with similar partition coefficients (Bau et al., 1996; Voigt et al., 2017), seawater REEs patterns including Ce anomaly could be recorded in marine carbonates and resistant to diagenesis alteration and dolomitization (Nothdurft et al., 2004; Li et al., 2019; Liu et al., 2019; Webb and Kamber, 2000). Thus, Ce anomaly values in marine carbonates have been demonstrated to provide continuous records of oxygen level changes in Earth history (Bellefroid et al., 2018; Liu et al., 2021; Wallace et al., 2017). REEs can also substitute for Ca in phosphate minerals such as apatite, and the seawater-like REE pattern extracted from phosphorites suggest that they can record the primary seawater REEs. In addition, Fe/Mn oxides, ion formations, and cherts are also used as seawater REE archives as REEs can be adsorbed onto these sediments without significant fractionation (Bau and Dulski, 1996; Derry and Jacobsen, 1990; Maliva et al., 2005; Planavsky et al., 2010; Siever, 1992; Shields and Stille, 2001).

REEs behave coherently as a group in various environments, and Cerium is the only REE that can be oxidized from trivalent state to tetravalent oxidation state, while other REEs behave as a coherent group and dissolve in seawater in trivalent state. This Ce oxidation process occurs rapidly on the surface of ferromanganese oxyhydroxides in shallow water driven by bacterial mediation and abiotic oxidation (Moffett, 1990, Moffett, 1994a, Moffett, 1994b; Takahashi et al., 2007; Tanaka et al., 2010). Tetravalent Ce is insoluble and is preferentially scavenged onto Fe-Mn oxyhydroxides, leaving the residual seawater depleted in Ce relative to other dissolved REEs after concentration normalization to the UCC (Upper Continental Crust) (Liu et al., 2019; Liu et al., 2021) or PAAS (Post Archean Australian Shale) (German and Elderfield, 1990). Such relative depletion in normalized Ce concentration is referred as the negative Ce anomaly ($Ce/Ce^* = Ce \times Nd/Pr^2$) (Lawrence et al., 2006; Lawrence and Kamber, 2006), and is ubiquitous in the well-oxidized open ocean. In contrast, REE distribution in modern anoxic water (e.g., Cariaco Trench, Black Sea) usually displays no Ce anomaly or slightly positive Ce anomaly (German and Elderfield, 1990; German et al., 1991). This suggests Ce oxidation is suppressed in the absence of oxygen, and slightly positive Ce anomaly indicates Ce (IV) can be reduced to dissolved state after the scavenging in the reducing environment (Tostevin et al., 2016). Therefore, distinct Ce anomaly values in seawater could indicate their redox environments (e.g., oxic versus anoxic).

Despite that the presence and absence of oxygen generates distinctive Ce anomaly signatures, the large variations of Ce anomalies in the modern ocean have attributed to other factors including cycling of Fe and Mn, ocean circulation and terrestrial inputs such as groundwater and dust (Hathorne et al., 2015; Seo and Kim, 2020; Wang et al., 2022; Zhang and Shields, 2022). Moreover, the quantitative relationship of Ce anomaly on the oceanic dissolved oxygen have not been systematically investigated, especially from a thermodynamic perspective. For example, Liu et al. (1988) developed a thermodynamic model to describe Ce concentrations with the CO_2 and O_2 partial pressure of the upper oceans. This model requires oceanic Ca concentration that challenges its potential paleo-oceanographic application. Moreover, this model only considered Ce-PO_4^{3-} complexation, whereas seawater trivalent Ce is mainly complexed with CO_3^{2-} or HCO_3^- (Byrne and Kim, 1993; Lee and Byrne, 1993, Lee and Byrne, 1992). It is known that carbonate complexations in Ce $(CO_3)^+$ or $Ce(CO_3)_2^-$ become predominant at near-neutral to alkaline pH (Cantrell and Byrne, 1987; Nakada et al., 2017). In addition, the model in (Liu et al., 1988) was calibrated using only one anoxic basin while lacks calibration in the oxic settings.

The objective of this study is to establish the quantitative relationship between seawater Ce concentration/Ce anomaly and the dissolved oxygen contents using thermodynamics-based Ce oxidization modeling approach. Here we examine both carbonate and phosphate complexations and derive models with varying complexations of trivalent Ce and oxidation pathways. More importantly, the models are calibrated using observational data from two modern oceanic profiles, including an oxic open ocean and an anoxic basin.

2 Theoretical considerations

2.1 Compilation of thermodynamic data

The Ce oxidation model considers complexations of dissolved Ce^{3+} and the oxidation pathways. The dissolved Ce species in the seawater under a normal range of pe-pH conditions are summarized in Table 1. Most dissolved Ce (C_{Ce}) (81%) are consist of $Ce(CO_3)^+$ and $Ce(CO_3)_2^-$ (Cantrell and Byrne, 1987; Luo and Byrne, 2004) developed the formulations for the carbonate complexations of Ce^{3+}, and the equilibrium constants are at 10°C and 25°C, atmospheric pressure (Table 2):

$$Ce^{3+} + 2CO_3^{2-} = Ce(CO_3)_2^-$$
$$Ce^{3+} + CO_3^{2-} = CeCO_3^+$$
$$Ce^{3+} + 2HCO_3^- = Ce(CO_3)_2^- + 2H^+$$
$$Ce^{3+} + HCO_3^- = CeCO_3^+ + H^+$$

The first and second stability constants for the Ce carbonate complexes in seawater are ~$10^{5.0}$ and $10^{8.4}$ (Cantrell and Byrne,

TABLE 1 The speciation of Ce in seawater (S=35, T=25°C, pH=8.2, Total CO_2 = 1.95 mmol/L [for data in de Baar et al. (1988)].

Dissolved species	% of total Ce	Activity coefficient	Relative activity	Reference
Ce^{3+}	3.53	0.049	0.173	de Baar et al. (1988)
$CeHCO_3^{2+}$	0.178	0.289	0.052	
$CeCO_3^{+}$	56.5	0.794	44.9	
$Ce(CO_3)_2^{-}$	24.2	0.648	15.7	
$Ce(OH)_2^{+}$	5.91	0.289	1.71	
$Ce(OH)_2^{+}$	5.33	0.794	4.23	
$Ce(OH)_3^{0}$	0.166	1.0	0.166	
$CeSO_4^{+}$	1.88	0.794	1.49	
$Ce(SO_4)_2^{-}$	0.245	0.648	0.159	
$CePO_4^{0}$	Less than 0.1	—	—	Liu and Byrne (1998)
$Ce(OH)_4$	0.126	—	—	Calculated based on Berger (2002)

TABLE 2 Selected equilibrium constants of reactions at 25°C, atmospheric pressure.

No.	Reaction	Log β/log k	Log K^0	References
(1)	$Ce^{3+} + 2CO_3^{2-} = Ce(CO_3)_2^{-}$	9.26 (I = 0.68)	17.53	Cantrell and Byrne (1987)
(2)	$Ce^{3+} + CO_3^{2-} = CeCO_3^{+}$	5.41 (I = 0.68)	7.61	Cantrell and Byrne (1987)
		6.95		Millero (1992)
			7.31	Liu and Byrne (1995)
			7.40	Lee and Byrne (1993)
			7.43	
(3)	$Ce^{3+} + 2HCO_3^{-} = Ce(CO_3)_2^{-} + 2H^{+}$	7.78 (I = 0.68)	8.9	Calculated based on Luo and Byrne (2004)
(4)	$Ce^{3+} + HCO_3^{-} = CeCO_3^{+} + H^{+}$	2.34 (I = 0.68)	3.27	Calculated based on Luo and Byrne (2004)
(5)	$Ce^{3+} + PO_4^{3-} = CePO_4^{0}$		18.5	Ehrlich (1968)
			16	Byrne and Bingler (1989)
(6)	$Ce^{3+} + 4OH^{-} = Ce(OH)_4 + e^{-}$	29.0		Liu et al. (1988)
(7)	$Ce(OH)_4 + PO_4^{3-} + e^{-} = CePO_4^{0} + 4OH^{-}$	10.5		Liu et al. (1988)
(8)	$Ce^{3+} = Ce^{4+} + e^{-}$	−21.6		Ehrlich (1968)
(9)	$Ce^{3+} + 2H_2O = CeO_2 + 4H^{+} + e^{-}$	−21.3		de Baar et al. (1988)
(10)	$Ce^{3+} + 4OH^{-} = Ce(OH)_4 + e^{-}$	50.6		Sillen and Martell (1964)
(11)	$Ce^{4+} + 4H_2O = Ce(OH)_4 + 4H^{+}$		−5.6	Sillen and Martell (1964)
(12)	$Ce^{4+} + 2H_2O = CeO_2 + 4H^{+}$		8.14	de Baar et al. (1988)
(14)	$Ce(OH)_4 = CeO_2 + 2H_2O$		13.56	de Baar et al. (1988)
(15)	$\frac{1}{2}H_2O = \frac{1}{4}O_2 + H^{+} + e^{-}$		−20.7	Millero et al. (2008)
(16)	$H_2O_2 = O_2 + 2H^{+} + 2e^{-}$		−23.0	Sillen and Martell (1964)
(17)	$H^{+} + OH^{-} = H_2O$		14.0	Rao et al. (1970)
(18)	$CePO_4^{0} + 3OH^{-} + \frac{1}{4}O_2 + \frac{1}{2}H_2O = PO_4^{3-} + Ce(OH)_4$		17.2	Calculated in this study
(19)	$CO_2 + H_2O = H_2CO_3$		−1.53	Millero et al. (2008)
(20)	$H_2CO_3 = HCO_3^{-} + H^{+}$	−6.1 (T=10°C)	−6.0	Riley and Skirrow (1975)
(21)	$HCO_3^{-} = CO_3^{2-} + H^{+}$		−9.11	
(22)	$CePO_4^{0} + \frac{1}{4}O_2 + \frac{3}{2}H_2O = PO_4^{3-} + 3H^{+} + CeO_2$		−17.9	Calculated in this study
(23)	$CeCO_3^{+} + \frac{3}{2}H_2O + \frac{1}{4}O_2 = HCO_3^{-} + 2H^{+} + CeO_2$		−2.94	Calculated in this study
(24)	$CeCO_3^{+} + \frac{3}{2}H_2O + \frac{1}{4}O_2 = CO_3^{2-} + 3H^{+} + CeO_2$		−7.91	Calculated in this study
(25)	$Ce(CO_3)_2^{-} + \frac{3}{2}H_2O + \frac{1}{4}O_2 = 2HCO_3^{-} + H^{+} + CeO_2$		−8.38	Calculated in this study
(26)	$Ce(CO_3)_2^{-} + \frac{3}{2}H_2O + \frac{1}{4}O_2 = 2CO_3^{2-} + 3H^{+} + CeO_2$		−9.86 (I=0.68)	Calculated in this study
			−18.13	

1987). The Ce^{3+} is also complexed extensively by PO_4^{3-} in seawater. The stability constant of $CePO_4^0$ is $10^{18.5}$ (Ehrlich, 1968) and 10^{16} (Byrne and Bingler, 1989), including the activity of $CePO_{4(aq)}$. $CePO_4^0$ consists less than 0.1% of total Ce^{3+}.

$$Ce^{3+} + PO_4^{3-} = CePO_4^0$$

The oxidation of Ce^{3+} to tetravalent Ce (Ce^{4+}) can be described in:

$$Ce^{3+} = Ce^{4+} + e^-$$
$$Ce^{4+} + 4OH^- = Ce(OH)_4$$
$$Ce^{3+} + 4OH^- = Ce(OH)_4 + e^-,\ E^0 = -1.71V$$

Notably, Ce^{3+} can hardly exist in seawater, but usually forms $Ce(OH)_4$, therefore Liu et al. (1988) derived the following reactions using hydroxylation of Ce^{3+}:

$$Ce(OH)_4 + PO_4^{3-} + e^- = CePO_4^0 + 4OH^-,\ E^0 = 0.62V$$

However, $Ce(OH)_4$ is not stable in seawater and quickly transforms to CeO_2:

$$Ce(OH)_4 = CeO_2 + 2H_2O$$

Seawater is a very complex oxygenated solution. Here we use dissolved oxygen as a strong oxidizing agent in seawater because the oxidation of Ce^{3+} requires the presence of oxygen. The E_h can be expressed by the half-cell reaction (Sillen and Martell, 1964; Millero, 1992):

$$\frac{1}{2}H_2O = \frac{1}{4}O_2 + H^+ + e^-, E_h^0 = 0.62V$$
$$H_2O_2 = O_2 + 2H^+ + 2e^-, K = 10^{-23.0}$$

2.2 Derivation of equations for Ce oxidation

2.2.1 Complexation with phosphorus ion

The models derived from phosphorus complexation is modified from the formulations in Liu et al. (1988). We derive Model #1 using reactions (5) (8) (10) (15) (17) (Table 2) and have:

$$CePO_4^0 3OH^- + \frac{1}{4}O_2 + \frac{1}{2}H_2O = PO_4^{3-} + Ce(OH)_4, logK = 17.2$$

$$\log\{CePO_4^0\} = 24.8 + \log\{PO_4^{3-}\} + \log\{Ce(OH)_4\} - 3pH - 0.25\log(pO_2)$$

Liu et al. (1988) calculated that $a_{Ce(OH)_4} \sim 1.6 \times 10^{-4}$. Based on Table 2, $CePO_4^0$ consists less than 0.1% of total dissolved Ce (C_{Ce}). Therefore, we use 0.001 C_{Ce} to replace $\{CePO_4^0\}$ and obtain (Model #1):

$$\log\{0.001{*}C_{Ce}\} \sim log\{CePO_4^0\} = 21 + \log\{PO_4^{3-}\} - 3pH - 0.25\,log(pO_2)$$

To avoid using the activity of Ce(OH)4, we add reaction (14) and have the following (Model #2):

$$CePO_4^0 + 3OH^- + \frac{1}{4}O_2 = CeO_2 + \frac{3}{2}H_2O,\ logK = 30.58$$
$$\log\{0.001{*}C_{Ce}\} \sim \{CePO_4^0\} = 11.42 + \log\{PO_4^{3-}\} - 3pH - 0.25\,log(pO_2)$$

We can also use reaction (9) (Table 2) instead of (5) (8) (14) (Model #3):

$$CePO_4^0 + \frac{1}{4}O_2 + \frac{3}{2}H_2O = PO_4^{3-} + 3H^+ + CeO_2,\ logk = -17.9$$
$$\log\{0.001{*}C_{Ce}\} \sim \{CePO_4^0\} = 17.9 + \log\{PO_4^{3-}\} - 3pH - 0.25\,log(pO_2)$$

The above models used equilibrium and stability constants at 25°C, and E_h^0 for reaction (15) (Table 2) is under ideal conditions and a modified E^0 needs to be calculated at 10°C,

$$H_2O = \frac{1}{2}O_2 + 2H^+ + 2e^-, E^0 = 0.84$$

For seawater at 10°C, f(O_2) = 0.2, pH= 8.1, We have,

$$Eh = E^0 + \frac{0.056}{4}\ log(pO_2) + 0.056\log\{H^+\}$$

When $pO_2 = 0.2$, $pH = 8.1$, $T = 10℃$, $Eh = 0.38V$, substituting into the

$$0.38 = 0.84 + 0.014\,logpO_2 + 0.056\log\{H^+\} \quad (1)$$

$$\text{For reaction (6), } \mathbf{K} = \frac{\{CePO_4^0\}\cdot\{OH^-\}^4}{\{Ce(OH)_4\}\cdot\{PO_4^{3-}\}.\{e^-\}}$$

$$\text{Thus, } \{e^-\} = \frac{\{CePO_4^0\}\cdot\{OH^-\}^4}{\{Ce(OH)_4\}\cdot\{PO_4^{3-}\}.K}$$

$$-log\{e^-\} = pe = logK + log\frac{\{Ce(OH)_4\}.\{PO_4^{3-}\}}{\{CePO_4^0\}.\{OH^-\}^4}$$

Therefore,

$$Eh = \frac{2.3RT}{F} = 0.056\,pe\ (T = 10℃)$$
$$= -0.62 + 0.056log\frac{\{Ce(OH)_4\}.\{PO_4^{3-}\}}{\{CePO_4^0\}.\{OH^-\}^4} \quad (2)$$

For $K(CePO_4^0) = 10^{-16}$, measured $\{Ce(OH)_4\} = \sim 1.6 \times 10^{-4}$, and substituting (Eq. 1) into (Eq. 2), we obtain

$$log\{CePO_4^0\} = 24.9 + log\{PO_4^{3-}\} - 0.25\log(pO_2) - 3pH$$

For $K(CePO_4^0) = 10^{-18.52}$, $\{Ce(OH)_4\} = \sim 10^{-6}$, we get (Model #4)

$$\log\{0.001^{*}C_{Ce}\} \sim log\{CePO_4^0\} = 24.9 + \log\{PO_4^{3-}\} - 3pH - 0.25\,log\,(pO_2)$$

When $\{Ce(OH)_4\} = \sim 1.6 \times 10^{-4}$, we obtain (Model #5)

$$\log\{0.001{*}C_{Ce}\} \sim log\{CePO_4^0\} = 22.6 + log\{PO_4^{3-}\} - 0.25\log(pO_2) - 3pH$$

In Liu et al. (1988), an average of $\{PO_4^{3-}\} = 10^{-9.4}$ in seawater was used as a substitute for $\{PO_4^{-3}\}$ in Model #5, therefore, we have (Model #6)

$$\log\{0.001{*}C_{Ce}\} \sim log\{CePO_4^0\} = 13.2 - 0.25log\,(pO_2) - 3pH$$

2.2.2 Complexation with carbonate ions

Using reactions (4), (9), (17), we can derive the following (Model #7):

$$CeCO_3^+ + \frac{3}{2}H_2O + \frac{1}{4}O_2 = HCO_3^- + 2H^+ + CeO_2,\ logK = -2.94$$

$$\log\{0.449{*}C_{Ce}\}{\sim}\log\{CeCO_3^+\} = 2.94 + \log\{HCO_3^-\} - 2pH - 0.25\,log\,(pO_2)$$

From reactions (2) (9) and (17) (Table 2), we obtain

$$CeCO_3^+ + \frac{3}{2}H_2O + \frac{1}{4}O_2 = CO_3^{2-} + 3H^+ + CeO_2,\ logK = -7.91$$

$$\log\{0.449{*}C_{Ce}\}{\sim}\log\{CeCO_3^+\} = 7.91 + \log\{CO_3^{2-}\} - 3pH - 0.25log\,(pO_2)$$

(Model#8)

From reactions (3) (9) and (17) (Table 2), we obtain (Model #9)

$$Ce(CO_3)_2^- + \frac{3}{2}H_2O + \frac{1}{4}O_2 = 2HCO_3^- + H^+ + CeO_2, logK = -8.38$$

$$\log\{0.157{*}C_{Ce}\} \sim \log\{Ce(CO_3)_2^-\} = 8.38 + 2\log\{HCO_3^-\} - pH - 0.25\log(pO_2)$$

From reactions (1) (9) (15) and (16), we get the followings:

$$Ce(CO_3)_2^- + \frac{3}{2}H_2O + \frac{1}{4}O_2 = 2CO_3^{2-} + 3H^+ + CeO_2,$$

$$logK = -9.86\ (I = 0.68), logK = -18.13\ (I = 0)$$

For I = 0.68, (Model #10)

$$\log\{0.157{*}C_{Ce}\}{\sim}\log\{Ce(CO_3)_2^-\} = 9.86 + 2\log\{CO_3^{2-}\} - 3pH - 0.25log\,(pO_2)$$

For I = 0, (Model #11)

$$\log\{0.157{*}C_{Ce}\} \sim \log\{Ce(CO_3)_2^-\} = 18.13 + 2\log\{CO_3^{2-}\} - 3pH - 0.25\,log\,(pO_2)$$

Accordingly, eleven derived Ce oxidation models are derived and listed in Table 3 and can be summarized as follows:

$$\log(\gamma_i C_{Ce}) = K - \frac{1}{4}\log(pO_2) + \partial_i\log\{\mathcal{X}_i\} - \beta_i pH \quad (3)$$

C_{Ce} represents total dissolved Ce in seawater, and γ_i represents the relative activity coefficient for trivalent Ce species including $CePO_4^0$, $CeCO_3^+$, and $Ce(CO_3)_2^-$. $(\partial_i, \mathcal{X}_i)$ are expressed as $(1, PO_4^{3-})$, $(1, HCO_3^-)$, or $(2, CO_3^{2-})$. β_i is one, two or three, depends on each Ce complexation reaction. Therefore, we can derive the general relationships between Ce concentration (C_{Ce}) with pO_2 and pH as follows:

$$C_{Ce} \sim \frac{1}{\{pO_2\}^{\frac{1}{4}}}$$

$$C_{Ce} \sim \mathcal{X}_i^{\partial_i}$$

$$log\,(C_{Ce}) \sim -\beta_i pH$$

Assuming other REEs in the water column are not affected by dissolved oxygen, then Ce anomaly mainly reflects changes in C_{Ce}. Thus, we can use the following relationship to quantify changes in pO_2, pH, and complexation ligands such as PO_4^{3-}:

$$\frac{Ce}{Ce^*} \sim C_{Ce} \sim \frac{1}{\{pO_2\}^{\frac{1}{4}}} \quad (4)$$

$$\frac{Ce}{Ce^*} \sim C_{Ce} \sim \mathcal{X}_i^{\partial_i} \quad (5)$$

$$\frac{Ce}{Ce^*} \sim C_{Ce} \sim \{H^+\}^{\beta_i} \quad (6)$$

2.3 Sensitivity test

2.3.1 Ce anomalies in the modern ocean

Assuming dissolved free oxygen is the oxidizer for seawater Ce^{3+}, all the derived models show the same relationship between Ce concentration and dissolved oxygen ($\frac{Ce}{Ce^*} \sim C_{Ce} \sim \frac{1}{\{pO_2\}^{\frac{1}{4}}}$). To evaluate this relationship, we compiled rare earth element concentrations in various vertical seawater profiles including South Pacific Ocean (Alibo and Nozaki, 1999; Molina-Kescher et al., 2014; Zhang and Nozaki, 1996), North Pacific Ocean (Zhang and Nozaki, 1998), West Pacific (Behrens et al., 2018) northeastern Indian Ocean (Nozaki and Alibo, 2003a), South Indian Ocean (Nozaki and Alibo, 2003b), South China Sea (Alibo and Nozaki, 2000), tropical South Pacific Ocean (Molina-Kescher et al., 2018), Southeast Atlantic Ocean (Garcia-Solsona et al., 2014), tropical South Atlantic Ocean (Zheng et al., 2016), tropical Atlantic Ocean (Tachikawa et al., 1999), and the Black Sea (German et al., 1991). Ce anomaly values are calculated using $Ce/Ce^* = Ce_N \times Nd_N/Pr_N^2$ (N means all the concentrations are normalized to the Upper Continental Crust following the approach in Cao et al. (2020) (Figure 1). It was suggested by de Baar et al. (1991) that La is not scavenged

TABLE 3 Derive equations for Ce oxidation model.

Model number	Equation
Complexation with phosphorus ion	
1	$\log\{0.001{*}C_{Ce}\} \sim log\{CePO_4^0\} = 21 + \log\{PO_4^{3-}\} - 3pH - 0.25\log(pO_2)$
2	$\log\{0.001{*}C_{Ce}\} \sim \{CePO_4^0\} = 11.42 + \log\{PO_4^{3-}\} - 3pH - 0.25\log(pO_2)$
3	$log\{0.001{*}C_{Ce}\} \sim \{CePO_4^0\} = 17.9 + log\{PO_4^{3-}\} - 3pH - 0.25\log(pO_2)$
4	$\log\{0.001{*}C_{Ce}\} \sim log\{CePO_4^0\} = 24.9 + \log\{PO_4^{3-}\} - 3pH - 0.25\log(pO_2)$
5	$\log\{0.001{*}C_{Ce}\} \sim log\{CePO_4^0\} = 22.6 + log\{PO_4^{3-}\} - 0.25\log(pO_2) - 3pH$
6	$log\{0.001{*}C_{Ce}\} \sim log\{CePO_4^0\} = 13.2 - 0.25\,log(pO_2) - 3pH$
Complexation with carbonate ion	
7	$\log\{0.449{*}C_{Ce}\} \sim log\{CeCO_3^+\} = 2.94 + \log\{HCO_3^-\} - 2pH - 0.25\log(pO_2)$
8	$\log\{0.449{*}C_{Ce}\} \sim log\{CeCO_3^+\} = 7.91 + \log\{CO_3^{2-}\} - 3pH - 0.25\log(pO_2)$
9	$\log\{0.157{*}C_{Ce}\} \sim log\{Ce(CO_3)_2^-\} = 8.38 + 2\log\{HCO_3^-\} - pH - 0.25\log(pO_2)$
10	$\log\{0.157{*}C_{Ce}\} \sim log\{Ce(CO_3)_2^-\} = 9.86 + 2\log\{CO_3^{2-}\} - 3pH - 0.25\log(pO_2)$
11	$\log\{0.157{*}C_{Ce}\} \sim log\{Ce(CO_3)_2^-\} = 18.13 + 2\log\{CO_3^{2-}\} - 3pH - 0.25\log(pO_2)$

strongly and is desorbed to a greater extent, therefore La should be not be used to quantify the Ce anomalies because the La often show positive anomaly in seawater (Lawrence and Kamber, 2006). However, Pr concentration was not measured in the Black Sea in German et al., 1991), thus we use Ce/Ce* = Ce × Nd/La^2 to calculate the Ce anomaly.

The compiled Ce anomalies show less variations below 500 m, and majority of the Ce anomaly values fall within 0–0.4, corresponding to oxidized seawater. The upper ocean (<500 m) has larger variations but most Ce anomaly values are lower than 1.0 except for some datapoints sampled from the surface water of South Pacific Ocean, and deep water in West Pacific. These samples exhibit Ce anomaly values larger than 1, but the *in-situ* dissolved oxygen levels in these sampling areas vary from 1 ml/L to 5 ml/L, which is still considered to be oxic. The relatively higher Ce anomalies in oxic water are possibly resulted from higher Ce concentration or lower Nd, Pr concentrations. The higher Ce concentration can due to uncertainties in Ce concentration measurement (de Baar et al., 1991; Sholkovitz and Schneider, 1991; Zhang and Nozaki, 1996) or inputs with no negative Ce anomaly from rivers, groundwaters and dust (Behrens et al., 2018). Nd is conservative in the intermediate water. However, low Nd concentration has been found to be correlated with high salinity water mass of Pacific Tropical Water (Behrens et al., 2018). In tropical oceans, processes other than redox change including scavenging input and ocean circulation can produce high Ce anomalies (>1).

Further, we plot the compiled Ce anomaly against $1/(pO_2)^{0.25}$ (Figure 2), where we show that high dissolved oxygen contents ($pO_2 > 0.05$) correspond to Ce anomaly values below 0.4, except for few outliers. Whereas as pO_2 decreases below 0.01, the Ce anomaly value progressively increases to 1.0, suggesting that under suboxic to anoxic environment the Ce anomaly values are sensitive to minor changes in dissolved oxygen concentration. The correspondences of Ce anomaly to dissolved oxygen concentration in suboxic-anoxic water column suggest that when oxygen is present, Ce anomaly is mainly controlled by the oxidation of trivalent Ce and preferential scavenging of tetravalent Ce relative to other trivalent REEs. While under suboxic-anoxic environment, the positive Ce anomaly could be enhanced by reduction of tetravalent Ce and released from Fe-Mn oxides/hydroxides (German et al., 1991). In the oxic water column, however, absolute Ce anomaly value does not correlate with dissolved oxygen level. Therefore, under oxic environment, dissolved oxygen no longer has dominant control on the Ce anomalies. The variations of Ce anomaly of oxic water mass are resulted from incoherent adsorption and desorption of individual REEs. Ocean particulates, especially Mn oxides and organic matters, preferentially scavenge light REEs, particularly Ce (Zhang and Nozaki, 1996). This implies that Ce anomalies between 0 and 0.4 cannot be related to variations in dissolved oxygen contents.

2.3.2 Model validation

We further calibrated the derived models in two vertical water column profiles: the South China Sea (Alibo and Nozaki, 2000) and the Black Sea (German et al., 1991), representing oxic open-ocean setting and anoxic–euxinic basin, respectively. Temperature, dissolved oxygen (annual average), and phosphate concentrations for the depth profiles were compiled from previous studies as well as estimated according to the WOA 13 (World Ocean Atlas 13) using the Ocean Data View navigation. In addition, alkalinity and pH data were obtained from NOAA (National Oceanic and Atmospheric Administration) (Yaitskaya, 2011) (Supplementary Table S2).

The South China Sea is a large marginal sea and is rapidly flushed by the Pacific Ocean (Alibo and Nozaki, 2000). The dissolved oxygen gradually decreases downwards and reaches the

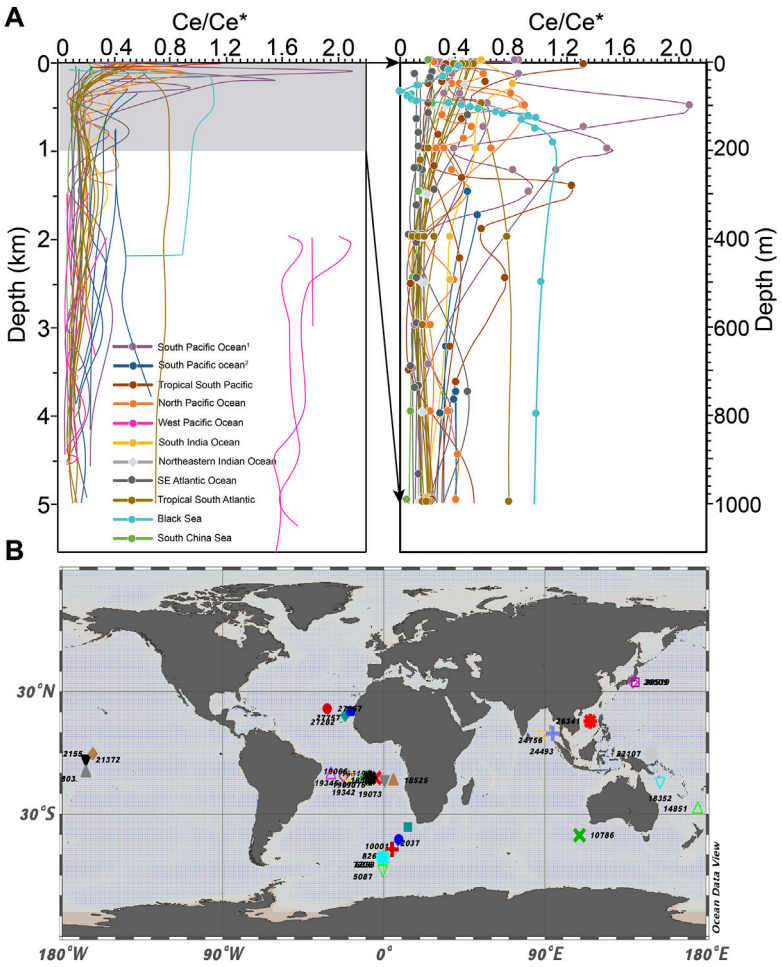

FIGURE 1
(A) Compilations of modern ocean vertical Ce anomaly profiles (Date sources are included in Methods and Materials). The right panel of **(A)** is enlarged modern ocean depth profiles of the Ce anomaly, displaying only 0–1 km *x*-axis is in log scale. **(B)** World map of station numbers used to extract annual dissolved oxygen concentrations in the WOA 13. Ce anomalies are recalculated in this study using $Ce/Ce^* = Ce \times Pr/Nd^2$ with compiled REE concentrations. For the Black Sea, we use $Ce/Ce^* = Ce \times La/Nd^2$ to calculate the Ce anomaly because Pr concentration was not measured in that study.

minimum of 2 ml/L, then slightly increases to 3 ml/L towards the bottom (Figure 3A). Meanwhile, Ce anomaly reaches the minimum at 1,000 m and stays constant throughout the vertical profile. The Black Sea is a stable anoxic basin where dissolved oxygen level is down to 1 μmol/L near the O_2/H_2S interface (1,000–1,200 m) (Rue et al., 1997). This trend is in contrast to both Ce concentrations and Ce anomalies (Figure 3B). From the sea surface to about 75 m, Ce anomaly decreases from 0.5 to 0.1. Below 75 m, with progressive loss of dissolved oxygen in the water column, Ce anomaly increases from 0.1 to ~1.0, stabilizing between 0.8 and 1.0 below the O_2/H_2S interface. Below the interface, Ce anomaly maintains above 0.8 except for the deepest sample ($Ce/Ce* = 0.4$). This anomalous feature can be explained by the intrusion of a small amount of well-oxygenated water into the ferruginous water column (German and Elderfield, 1990). Above the oxic/suboxic boundary, the oxidative precipitation of Ce during scavenging leads to depletion of trivalent Ce in the solution. Below the oxic/suboxic interface, as dissolved Mn and Fe concentrations increase, the release of REEs into solution elevate the dissolved Ce concentration while reduce the pronounced Ce-depletion (German and Elderfield, 1989).

We used dissolved oxygen, phosphate concentration, pH, and alkalinity to calculate the total dissolved Ce concentration using Models #1–#11 and compared the calculated values to the measured concentrations. We use the CO_2 equilibrium system to calculate the activity of CO_3^- and HCO_3^-. For reaction (19) (Table 2), K_H stands for the equilibrium constant of association of H_2CO_3 (aq):

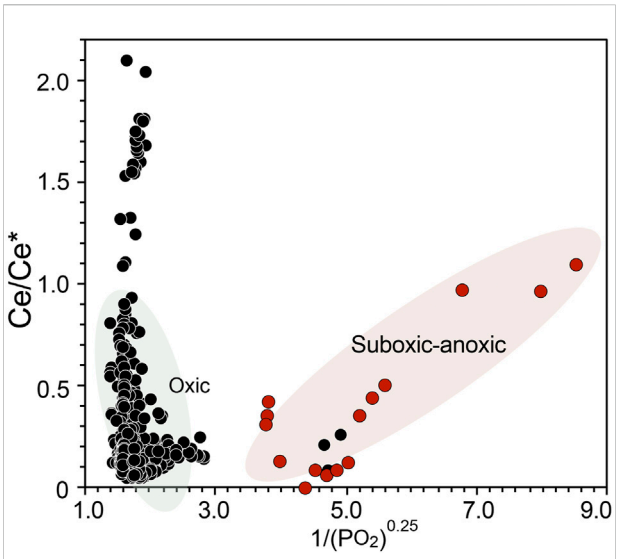

FIGURE 2
A cross-plot of compiled Ce anomalies and $1/(pO_2)^{0.25}$. Dissolved oxygen concentrations are compiled from references listed in figure caption of Figure 1 as well as estimated by extracting annual average dissolved oxygen contents at each station utilizing WOA 13. Black circles indicate samples in oxic environments while red circles represent samples under suboxic-anoxic environments.

$$CO_2 + H_2O = H_2CO_3\ (aq)$$

$$K_H = \frac{\{H_2CO_3\,(aq)\}}{p_{CO_2}\{H_2O\ (l)\}} = \frac{\{H_2CO_3\,(aq)\}}{p_{CO_2}\gamma_{H_2O}\chi_{H_2O}} = \frac{\{H_2CO_3\,(aq)\}}{p_{CO_2}\,0.981}$$

For reaction (20) (Table 2), the equilibrium constants for dissociation of H_2CO_3 (aq) can be expressed by K_1 as:

$$H_2CO_3\ (aq) = HCO_3^- + H^+$$

$$K_1 = \frac{\{HCO_3^-\}\{H^+\}}{\{H_2CO_3\,(aq)\}} = \frac{\{HCO_3^-\}\{H^+\}}{0.981\,K_H\,p_{CO_2}}$$

From here, we can calculate:

$$\{HCO_3^-\} = \frac{0.981\,K_1\,K_H\,p_{CO_2}}{\{H^+\}}$$

Similarly, for reaction (21) (Table 2), the equilibrium constants for dissociation of HCO_3^- (aq) can be expressed by K_2 as:

$$HCO_3^- = CO_3^{2-} + H^+$$

$$K_2 = \frac{\{CO_3^{2-}\}\{H^+\}}{\{HCO_3^-\,(aq)\}} = \frac{\{CO_3^{2-}\}\{H^+\}^2}{0.981\,K_1\,K_H\,p_{CO_2}}$$

$$\{CO_3^{2-}\} = \frac{0.981\,K_1\,K_2\,K_H\,p_{CO_2}}{\{K^+\}^2}$$

We use CA to represent alkalinity and TA for total dissolved carbon dioxide,

$$CA(\{HCO_3^-\} + \{CO_3^{2-}\}) \approx 0.958TA(\{HCO_3^-\} + \{CO_3^{2-}\} + \{H_2CO_3\,(aq)\})$$

$$\partial 1 = \frac{\{HCO_3^-\}}{TA} = \left[\frac{\{H^+\}}{K_1} + \frac{K_2}{\{H^+\}} + 1\right]^{-1}$$

$$\partial 2 = \frac{\{CO_3^{2-}\}}{TA} = \left[\frac{\{H^+\}^2}{K_1K_2} + \frac{\{H^+\}}{K_2} + 1\right]^{-1}$$

C_{Ce} is calculated using Models #1–11 derived above and compared to the reported values in the two vertical profiles. The offsets of C_{Ce} between model calculated and measure are expressed as (calculated Ce concentration/measured Ce concentration − 1) × 100%. In both profiles, Model #3 ($log\{0.001{*}C_{Ce}\} \sim \{CePO_4^0\} = 17.9 + log\{PO_4^{3-}\} - 3pH - 0.25\,log\,(pO_2)$) shows the smallest offset of

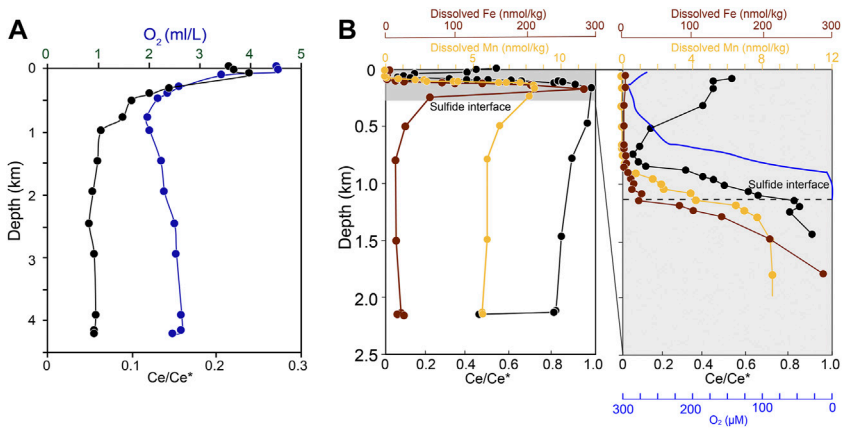

FIGURE 3
Vertical profiles of dissolved oxygen content (blue) and Ce anomaly (Ce/Ce* = Ce*Nd/Pr²) (black) for one station in the **(A)** South China Sea (Alibo and Nozaki, 2000) and **(B)** the Black sea (German et al., 1991). Here we use Ce/Ce* = Ce × La/Nd² to calculate the Ce anomaly in the Black Sea because Pr concentration was not measured.

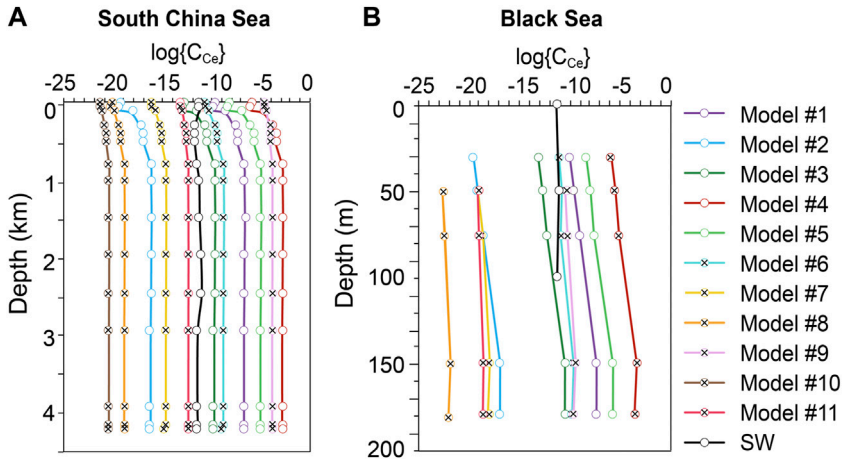

FIGURE 4
Predicted Log{C_{Ce}} values by models #1–#11 and previously measured values reported as Log{C_{Ce}} in **(A)** South China Sea, and **(B)** Black Sea. Parameters needed for model calculation are presented in the Supplementary Tables S1, S2.

C_{Ce} (Figure 4). For the South China Sea, the offsets calculated using Model #3 are smaller than 100% in 0–100 m, and increase 50 folds downwards due to the large variations in phosphate concentration. However, the alkalinity does not vary significantly within the vertical profile, and models based on carbonate complexations (Model #7–Model #11) have constant C_{Ce} offsets at different depths. The C_{Ce} offsets in the other well-validated model, namely Model #11, are within −80% to −100%. For the Black Sea, C_{Ce} offsets in Model #3 vary from −48% to −95%. However, Model #11 does not work well in this profile because alkalinity is about 0.1% of that in the open ocean. At 150 m and 200 m where oxygen almost disappeared, Model #9 shows relatively small offsets, 130% and 213%, respectively. Larger offsets seen in other models may be caused by influences from temperature, thermodynamic data quality, or other processes controlling Ce concentration including dust input and sediment adsorption/desorption processes.

3 Discussion

The sensitivity test suggests that under oxic environment, the exact Ce anomaly values does not correspond to a certain dissolved oxygen content, however, the increase in Ce anomaly can semi-quantitatively constrain the deoxygenation level during the transition from oxic to suboxic-anoxic environment, e.g., during oceanic deoxygenation events. Therefore, we define the $f_{Ce/Ce*}$ as the magnitude of increase in Ce anomaly divided by the starting Ce anomaly. Similarly, we use fO_2 and $f\mathcal{X}_i$ to describe the amount of change in dissolved oxygen level, and carbonate/phosphate ions, respectively. The pH change is expressed as ΔpH, meaning the pH increase/decrease after subtracting the starting pH. For example, when Ce anomaly value of the depositional water column shift from 0.1 to 1.0, a.k.a, $f_{Ce/Ce}$ is 10. Using Eqs 4–6, we can calculate fO_2, $f\mathcal{X}_i$, and ΔpH (Figure 5). We find that dissolved oxygen concentrations, carbonate and phosphate concentrations are sensitive to $f_{Ce/Ce*}$. For example, using two well-calibrated models—Model #3 and Model #11, PO_4^{3-} would increase three folds and CO_3^{2-} would increase 1.5 folds corresponding to $f_{Ce/Ce*}$ = 10. The sensitivity of ambient pH to Ce anomaly change is the smallest in Model #3, Model #6 and Model #11, for whom are the best calibrated models using the South China Sea and the Black Sea data. A decline of 0.3 in pH is observed using these models when $f_{Ce/Ce*}$ = 10. Model #9 has the largest sensitivity of ambient pH to $f_{Ce/Ce*}$, where pH can decrease by over 1.0 corresponds to $f_{Ce/Ce*}$ = 10.

Decrease in temperature may influence the complexations of Ce^{3+} (Cantrell and Byrne, 1987). For example, hydrolysis through the formation of $Ce(OH)_2^+$ is enhanced and formation of $Ce(CO_3)_2^-$ is reduced under 15°C relative to 25°C. However, modest temperature effect was reported: the overall Ce speciation at 15°C is found to be very similar to that at 25°C (Cantrell and Byrne, 1987). Decreases in temperature may also influence the stability constants for reactions. As we can see in Eq. 4, despite the equilibrium constants would change with temperature, the relationship between dissolved Ce concentration and other variables remains the same under different temperatures. Thus, we can use the relative Ce anomaly change during deoxygenation event to estimate the extent oxygen loss in the ocean, and potentially estimate changes in pH, phosphate concentration, and alkalinity.

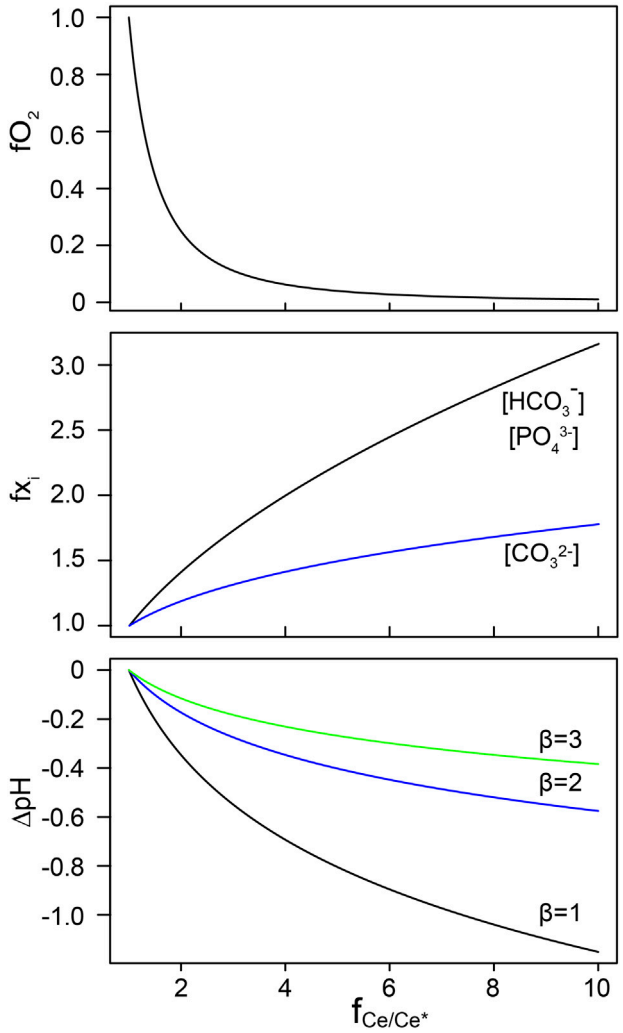

FIGURE 5
Model outputs of derived Ce oxidation models in Table 2. We use fCe/Ce* to describe the magnitude/ratio of increase in Ce anomaly. The magnitude of change in dissolved oxygen level, carbonate and phosphate ions are expressed as fO_2 and f $\mathcal{X}_i$, respectively. The pH change is expressed as ΔpH, meaning the pH of increased Ce anomaly subtracting the starting pH.

Previous studies have demonstrated that reliable seawater Ce anomaly signals can be extracted from marine carbonates (Cao et al., 2020; Tostevin et al., 2016). Therefore, the model developed in this study can provide a first approximation of the extent of oxygen loss using Ce anomalies of pristine marine carbonates that recorded the oceanic deoxygenation events. For example, compilation of Ce anomaly in marine carbonates from 3.5 Ga to the present show shifts corresponding to the Great Oxidation Event and gives new estimates that the mid-Proterozoic atmospheric oxygen level is about 1% of the present atmospheric level assuming equilibrium between shallow seawater and atmosphere over millions of year time periods (Liu et al., 2021). This Ce oxidization model results serve as a complementary to the multi-proxy compilation of the oceanic oxygen change in response to climate change. However, the model results should be carefully interpreted due to the following reasons. First, as shown in the model, Ce anomaly could be significantly influenced by seawater pH. Therefore, oceanic Ce anomaly in deep time should account for the potential pH changes. Secondly, due to the short residence time of Ce, Nd, and Pr (less than 1,000 years), Ce anomaly values in carbonates that deposited in restricted areas may primarily reflect local redox conditions, thus have limited implication on global-scale redox conditions. The calculation of Ce anomaly involves Nd, Pr, and sometimes La, technically the concentration of these REEs would also cause variations in

Ce anomaly values. However, when using Ce anomaly as a local redox proxy, the increase in Ce anomaly value is mainly attributed to a higher Ce^{3+} concentration. In addition, Ce anomaly values show significant variations within (0–0.4) in fully oxidized water column, therefore within this range, the absolute Ce anomaly value does not necessarily reflect difference in dissolved oxygen content. Lastly, the modeling approach in this study assumes equilibrium attained, therefore the role of kinetics in fractionating REEs is suppressed, although the kinetic effect could be pronounced in dynamic marine environments. This model also does not apply to organic-rich waters and alkaline lakes where positive cerium anomaly was supressed in oxic environment (Davranche et al., 2005; Möller and Bau, 1993; Pourret et al., 2008, Pourret et al., 2007), or generated by ligand-driven oxidation in anoxic environment (Kraemer et al., 2017; Li and Liu, 2020). The microbial oxidation of trivalent Ce is beyond the scope of this study as well (Ohnuki et al., 2015). Nonetheless, this Ce oxidization model could be further tested and applied to quantify oceanic dissolve oxygen levels during various oceanic deoxygenation events, such as the OAE 2 (Oceanic Anoxic Event 2).

4 Conclusion

In this study, we developed and calibrated thermodynamic-based cerium oxidation models using changes in Ce anomaly values to quantify their dissolved oxygen levels in the modern ocean. We emphasize that these models are only suitable when the water column transits from oxic environment to anoxia or vice versa. Moreover, we notice that Ce anomaly value loses sensitivity in tracing small changes in dissolved oxygen content. Our sensitivity analyses indicate that Ce concentration is also impacted by pH, phosphorus concentration, and alkalinity. Therefore, the interpretation of deoxygenation and reoxygenation in seawater requires discussion of possible changes in all these factors that affect Ce anomaly in addition to its redox condition.

Data availability statement

The original contributions presented in the study are included in the article/Supplementary Material, further inquiries can be directed to the corresponding author.

Author contributions

CC and X-ML designed the research, CC performed the research, CC and X-ML wrote the manuscript with inputs from all authors.

Funding

CC acknowledge funding support from the National Natural Science Foundation of China (41991321) and the Graduate Research Fellowship from the The department of Earth, marine and environmental sciences, University of North Carolina at Chapel Hill. X-ML acknowledges funding support from the University of North Carolina at Chapel Hill.

Acknowledgments

Special thanks go to Marc Alperin and Larry Benninger for helpful discussion.

Conflict of interest

The authors declare that the research was conducted in the absence of any commercial or financial relationships that could be construed as a potential conflict of interest.

Publisher's note

Supplementary material

The Supplementary Material for this article can be found online at: https://www.frontiersin.org/articles/10.3389/feart.2022.927826/full#supplementary-material

References

Algeo, T. J., and Li, C. (2020). Redox classification and calibration of redox thresholds in sedimentary systems. *Geochimica Cosmochimica Acta* 287, 8–26. doi:10.1016/j.gca.2020.01.055

Algeo, T. J., and Tribovillard, N. (2009). Environmental analysis of paleoceanographic systems based on molybdenum-uranium covariation. *Chem. Geol.* 268, 211–225. doi:10.1016/j.chemgeo.2009.09.001

Alibo, D. S., and Nozaki, Y. (2000). Dissolved rare Earth elements in the South China Sea: Geochemical characterization of the water masses. *J. Geophys. Res.* 105, 28771–28783. doi:10.1029/1999JC000283

Alibo, D. S., and Nozaki, Y. (1999). Rare Earth elements in seawater: Particle association, shale-normalization, and Ce oxidation. *Geochimica Cosmochimica Acta* 63, 363–372. doi:10.1016/S0016-7037(98)00279-8

Bau, M., and Dulski, P. (1996). Distribution of yttrium and rare-Earth elements in the penge and kuruman iron-formations, transvaal supergroup, South Africa. *Precambrian Res.* 79, 37–55. doi:10.1016/0301-9268(95)00087-9

Bau, M., Koschinsky, A., Dulski, P., and Hein, J. R. (1996). Comparison of the partitioning behaviours of yttrium, rare Earth elements, and titanium between hydrogenetic marine ferromanganese crusts and seawater. *Geochimica Cosmochimica Acta* 60, 1709–1725. doi:10.1016/0016-7037(96)00063-4

Behrens, Melanie K., Pahnke, K., Paffrath, R., Schnetger, B., and Brumsack, H. J. (2018a). Rare Earth element distributions in the West Pacific: Trace element sources and conservative vs. non-conservative behavior. *Earth Planet. Sci. Lett.* 486, 166–177. doi:10.1016/j.epsl.2018.01.016

Behrens, Melanie K., Pahnke, K., Schnetger, B., and Brumsack, H. J. (2018b). Sources and processes affecting the distribution of dissolved Nd isotopes and concentrations in the West Pacific. *Geochimica Cosmochimica Acta* 222, 508–534. doi:10.1016/J.GCA.2017.11.008

Bellefroid, E. J., Hood, A. V. S., Hoffman, P. F., Thomas, M. D., Reinhard, C. T., and Planavsky, N. J. (2018). Constraints on Paleoproterozoic atmospheric oxygen levels. *Proc. Natl. Acad. Sci. U. S. A.* 115, 8104–8109. doi:10.1073/pnas.1806216115

Berger, W. H. (2002). Encyclopedia of ocean Sciences. *Eos Trans. AGU.* 83, 485. doi:10.1029/2002EO000342

Byrne, R. H., and Bingler, L. S. (1989). Comment on "cerium: A chemical tracer for paleo-oceanic redox conditions" by Y.-G. Liu, M. R. U. Miah and R. A. Schmitt. *Geochimica Cosmochimica Acta* 53, 1475–1476. doi:10.1016/0016-7037(89)90081-1

Byrne, R. H., and Kim, K.-H. (1993). Rare Earth precipitation and coprecipitation behavior: The limiting role of PO43− on dissolved rare Earth concentrations in seawater. *Geochimica Cosmochimica Acta* 57, 519–526. doi:10.1016/0016-7037(93)90364-3

Canfield, D. E. (2005). The early history of atmospheric oxygen: Homage to robert M. Garrels. *Annu. Rev. Earth Planet. Sci.* 33, 1–36. doi:10.1146/annurev.earth.33.092203.122711

Cantrell, K. J., and Byrne, R. H. (1987). Rare Earth element complexation by carbonate and oxalate ions. *Geochimica Cosmochimica Acta* 51, 597–605. doi:10.1016/0016-7037(87)90072-X

Cao, C., Liu, X.-M., Bataille, C. P., and Liu, C. (2020). What do Ce anomalies in marine carbonates really mean? A perspective from leaching experiments. *Chem. Geol.* 532, 119413. doi:10.1016/j.chemgeo.2019.119413

Chen, X., Tissot, F. L. H., Jansen, M. F., Bekker, A., Liu, C. X., Nie, N. X., et al. (2021). The uranium isotopic record of shales and carbonates through geologic time. *Geochimica Cosmochimica Acta* 300, 164–191. doi:10.1016/J.GCA.2021.01.040

Davranche, M., Pourret, O., Gruau, G., Dia, A., and le Coz-Bouhnik, M. (2005). Adsorption of REE(III)-humate complexes onto MnO2: Experimental evidence for cerium anomaly and lanthanide tetrad effect suppression. *Geochimica Cosmochimica Acta* 69, 4825–4835. doi:10.1016/j.gca.2005.06.005

de Baar, H. J. W., German, C. R., Elderfield, H., and van Gaans, P. (1988). Rare Earth element distributions in anoxic waters of the Cariaco Trench. *Geochimica Cosmochimica Acta* 52, 1203–1219. doi:10.1016/0016-7037(88)90275-X

de Baar, H. J. W., Schijf, J., and Byrne, R. H. (1991). Solution chemistry of the rare earth elements in seawater. *Eur. J. Solid State Inorg. Chem.* 28, 357–373.

Derry, L. A., and Jacobsen, S. B. (1990). The chemical evolution of Precambrian seawater: Evidence from REEs in banded iron formations. *Geochimica Cosmochimica Acta* 54, 2965–2977. doi:10.1016/0016-7037(90)90114-Z

Ehrlich, A. M. (1968). *Rare earth abundances in manganese nodules*. Cambridge: Massachusetts Inst of Tech.

Garcia-Solsona, E., Jeandel, C., Labatut, M., Lacan, F., Vance, D., Chavagnac, V., et al. (2014). Rare Earth elements and Nd isotopes tracing water mass mixing and particle-seawater interactions in the SE Atlantic. *Geochimica Cosmochimica Acta* 125, 351–372. doi:10.1016/j.gca.2013.10.009

German, C., and Elderfield, H. (1989). Rare Earth elements in Saanich Inlet, British Columbia, a seasonally anoxic basin. *Geochimica Cosmochimica Acta* 53, 2561–2571. doi:10.1016/0016-7037(89)90128-2

German, C. R., and Elderfield, H. (1990). Application of the Ce anomaly as a paleoredox indicator: The ground rules. *Paleoceanography* 5, 823–833. doi:10.1029/PA005i005p00823

German, C. R., Holliday, B. P., and Elderfield, H. (1991). Redox cycling of rare Earth elements in the suboxic zone of the Black Sea. *Geochimica Cosmochimica Acta* 55, 3553–3558. doi:10.1016/0016-7037(91)90055-A

Hathorne, E. C., Stichel, T., Brück, B., and Frank, M. (2015). Rare Earth element distribution in the Atlantic sector of the Southern Ocean: The balance between particle scavenging and vertical supply. *Mar. Chem.* 177, 157–171. doi:10.1016/J.MARCHEM.2015.03.011

Holland, H. D. (2006). The oxygenation of the atmosphere and oceans. *Phil. Trans. R. Soc. B* 361, 903–915. doi:10.1098/rstb.2006.1838

Kamber, B. S., Webb, G. E., and Gallagher, M. (2014). The rare Earth element signal in archaean microbial carbonate: Information on ocean redox and biogenicity. *J. Geol. Soc. Lond.* 171, 745–763. doi:10.1144/jgs2013-110

Kraemer, D., Tepe, N., Pourret, O., and Bau, M. (2017). Negative cerium anomalies in manganese (hydr)oxide precipitates due to cerium oxidation in the presence of dissolved siderophores. *Geochimica Cosmochimica Acta* 196, 197–208. doi:10.1016/j.gca.2016.09.018

Lawrence, M. G., Greig, A., Collerson, K. D., and Kamber, B. S. (2006). Rare earth element and yttrium variability in South east queensland waterways. *Aquat. Geochem.* 12, 39–72. doi:10.1007/s10498-005-4471-8

Lawrence, M. G., and Kamber, B. S. (2006). The behaviour of the rare Earth elements during estuarine mixing—Revisited. *Mar. Chem.* 100, 147–161. doi:10.1016/j.marchem.2005.11.007

Lee, J. H., and Byrne, R. H. (1993). Complexation of trivalent rare Earth elements (Ce, Eu, Gd, Tb, Yb) by carbonate ions. *Geochimica Cosmochimica Acta* 57, 295–302. doi:10.1016/0016-7037(93)90432-V

Lee, J. H., and Byrne, R. H. (1992). Examination of comparative rare Earth element complexation behavior using linear free-energy relationships. *Geochimica Cosmochimica Acta* 56, 1127–1137. doi:10.1016/0016-7037(92)90050-S

Li, F., Webb, G. E., Algeo, T. J., Kershaw, S., Lu, C., Oehlert, A. M., et al. (2019). Modern carbonate ooids preserve ambient aqueous REE signatures. *Chem. Geol.* 509, 163–177. doi:10.1016/j.chemgeo.2019.01.015

Li, W., and Liu, X. M. (2020). Mobilization and partitioning of rare Earth elements in the presence of humic acids and siderophores. *Chemosphere* 254, 126801. doi:10.1016/j.chemosphere.2020.126801

Ling, H.-F., Chen, X., Li, D., Wang, D., Shields-Zhou, G. A., and Zhu, M. (2013). Cerium anomaly variations in Ediacaran–earliest Cambrian carbonates from the Yangtze Gorges area, South China: Implications for oxygenation of coeval shallow seawater. *Precambrian Res.* 225, 110–127. doi:10.1016/j.precamres.2011.10.011

Liu, X.-M., Hardisty, D. S., Lyons, T. W., and Swart, P. K. (2019). Evaluating the fidelity of the cerium paleoredox tracer during variable carbonate diagenesis on the Great Bahamas Bank. *Geochimica Cosmochimica Acta* 248, 25–42. doi:10.1016/j.gca.2018.12.028

Liu, X.-M., Kah, L. C., Knoll, A. H., Cui, H., Kaufman, A. J., Shahar, A., et al. (2016). Tracing Earth's O2 evolution using Zn/Fe ratios in marine carbonates. *Geochem. Perspect. Lett.* 2, 24–34. doi:10.7185/geochemlet.1603

Liu, X.-M., Kah, L. C., Knoll, A. H., Cui, H., Wang, C., Bekker, A., et al. (2021). A persistently low level of atmospheric oxygen in Earth's middle age. *Nat. Commun.* 12, 351. doi:10.1038/s41467-020-20484-7

Liu, X., and Byrne, R. H. (1995). Comparative carbonate complexation of yttrium and gadolinium at 25 °C and 0.7 mol dm−3 ionic strength. *Mar. Chem.* 51, 213–221. doi:10.1016/0304-4203(95)00067-4

Liu, X., and Byrne, R. H. (1998). Comprehensive investigation of yttrium and rare Earth element complexation by carbonate ions Using ICP-mass spectrometry. *J. Solut. Chem.* 27, 803–815. doi:10.1023/a:1022677119835

Liu, Y.-G., Miah, M. R. U., and Schmitt, R. A. (1988). Cerium: A chemical tracer for paleo-oceanic redox conditions. *Geochimica Cosmochimica Acta* 52, 1361–1371. doi:10.1016/0016-7037(88)90207-4

Livermore, B. D., Dahl, T. W., Bizzarro, M., and Connelly, J. N. (2020). Uranium isotope compositions of biogenic carbonates – implications for U uptake in shells and the application of the paleo-ocean oxygenation proxy. *Geochimica Cosmochimica Acta* 287, 50–64. doi:10.1016/j.gca.2020.07.005

Lu, W., Ridgwell, A., Thomas, E., Hardisty, D. S., Luo, G., Algeo, T. J., et al. (2018). Late inception of a resiliently oxygenated upper ocean. *Science* 5372, 174–177. doi:10.1126/science.aar5372

Luo, Y. R., and Byrne, R. H. (2004). Carbonate complexation of yttrium and the rare Earth elements in natural waters. *Geochimica Cosmochimica Acta* 68, 691–699. doi:10.1016/S0016-7037(03)00495-2

Lyons, T. W., Reinhard, C. T., and Planavsky, N. J. (2014). The rise of oxygen in Earth's early ocean and atmosphere. *Nature* 506, 307–315. doi:10.1038/nature13068

Maliva, R. G., Knoll, A. H., and Simonson, B. M. (2005). Secular change in the Precambrian silica cycle: Insights from chert petrology. *Geol. Soc. Am. Bull.* 117, 835–845. doi:10.1130/B25555.1

Millero, F. J., Feistel, R., Wright, D. G., and McDougall, T. J. (2008). The composition of standard seawater and the definition of the reference-composition salinity scale. *Deep Sea Res. Part I Oceanogr. Res. Pap.* 55, 50–72. doi:10.1016/j.dsr.2007.10.001

Millero, F. J. (1992). Stability constants for the formation of rare Earth-inorganic complexes as a function of ionic strength. *Geochimica Cosmochimica Acta* 56, 3123–3132. doi:10.1016/0016-7037(92)90293-R

Moffett, J. W. (1994a). A radiotracer study of cerium and manganese uptake onto suspended particles in Chesapeake Bay. *Geochimica Cosmochimica Acta* 58, 695–703. doi:10.1016/0016-7037(94)90499-5

Moffett, J. W. (1990). Microbially mediated cerium oxidation in sea water. *Nature* 345, 421–423. doi:10.1038/345421a0

Moffett, J. W. (1994b). The relationship between cerium and manganese oxidation in the marine environment. *Limnol. Oceanogr.* 39, 1309–1318. doi:10.4319/lo.1994.39.6.1309

Molina-Kescher, M., Frank, M., and Hathorne, E. (2014). South Pacific dissolved Nd isotope compositions and rare Earth element distributions: Water mass mixing versus biogeochemical cycling. *Geochimica Cosmochimica Acta* 127, 171–189. doi:10.1016/j.gca.2013.11.038

Molina-Kescher, M., Hathorne, E. C., Osborne, A. H., Behrens, M. K., Kölling, M., Pahnke, K., et al. (2018). The influence of basaltic islands on the oceanic REE distribution: A case study from the tropical South pacific. *Front. Mar. Sci.* 5. doi:10.3389/fmars.2018.00050

Möller, P., and Bau, M. (1993). Rare-Earth patterns with positive cerium anomaly in alkaline waters from Lake Van, Turkey. *Earth Planet. Sci. Lett.* 117, 671–676. doi:10.1016/0012-821X(93)90110-U

Nakada, R., Tanaka, M., Tanimizu, M., and Takahashi, Y. (2017). Aqueous speciation is likely to control the stable isotopic fractionation of cerium at varying pH. *Geochimica Cosmochimica Acta* 218, 273–290. doi:10.1016/j.gca.2017.09.019

Nielsen, S. G., Rehkämper, M., and Prytulak, J. (2017). Investigation and application of thallium isotope fractionation. *Rev. Mineral. Geochem.* 82, 759–798. doi:10.2138/rmg.2017.82.18

Nothdurft, L. D., Webb, G. E., and Kamber, B. S. (2004). Rare Earth element geochemistry of late devonian reefal carbonates, canning basin, western Australia: Confirmation of a seawater REE proxy in ancient limestones. *Geochimica Cosmochimica Acta* 68, 263–283. doi:10.1016/S0016-7037(03)00422-8

Nozaki, Y., and Alibo, D. S. (2003b). Dissolved rare Earth elements in the Southern Ocean, southwest of Australia: Unique patterns compared to the South Atlantic data. *Geochem. J.* 37, 47–62. doi:10.2343/geochemj.37.47

Nozaki, Y., and Alibo, D. S. (2003a). Importance of vertical geochemical processes in controlling the oceanic profiles of dissolved rare Earth elements in the northeastern Indian Ocean. *Earth Planet. Sci. Lett.* 205, 155–172. doi:10.1016/S0012-821X(02)01027-0

Ohnuki, T., Jiang, M., Sakamoto, F., Kozai, N., Yamasaki, S., Yu, Q., et al. (2015). Sorption of trivalent cerium by a mixture of microbial cells and manganese oxides: Effect of microbial cells on the oxidation of trivalent cerium. *Geochimica Cosmochimica Acta* 163, 1–13. doi:10.1016/j.gca.2015.04.043

Ostrander, C. M., Nielsen, S. G., Owens, J. D., Kendall, B., Gordon, G. W., Romaniello, S. J., et al. (2019). Fully oxygenated water columns over continental shelves before the Great Oxidation Event. *Nat. Geosci.* 12, 186–191. doi:10.1038/s41561-019-0309-7

Planavsky, N., Bekker, A., Rouxel, O. J., Kamber, B., Hofmann, A., Knudsen, A., et al. (2010). Rare Earth Element and yttrium compositions of Archean and Paleoproterozoic Fe formations revisited: New perspectives on the significance and mechanisms of deposition. *Geochimica Cosmochimica Acta* 74, 6387–6405. doi:10.1016/J.GCA.2010.07.021

Planavsky, N. J., Reinhard, C. T., Wang, X., Thomson, D., McGoldrick, P., Rainbird, R. H., et al. (2014). Low Mid-Proterozoic atmospheric oxygen levels and the delayed rise of animals. *Science* 346, 635–638. doi:10.1126/science.1258410

Pourret, O., Davranche, M., Gruau, G., and Dia, A. (2007). Competition between humic acid and carbonates for rare Earth elements complexation. *J. Colloid Interface Sci.* 305, 25–31. doi:10.1016/j.jcis.2006.09.020

Pourret, O., Davranche, M., Gruau, G., and Dia, A. (2008). New insights into cerium anomalies in organic-rich alkaline waters. *Chem. Geol.* 251, 120–127. doi:10.1016/j.chemgeo.2008.03.002

Rao, V. K., Shanhani, C. J., and Rao, C. L., 1970. Studies on the phosphate complexes of actinium and lanthanum. *Radiochim. Acta.* 14, 31–34. doi:10.1524/ract.1970.14.1.31

Riley, J. P., and Skirrow, G. (Editors) (1975). *Chemical oceanography, v. 1.*, 2nd. (New York and London: Academic Press), xx + 606.

Rue, E. L., Smith, G. J., Cutter, G. A., and Bruland, K. W. (1997). The response of trace element redox couples to suboxic conditions in the water column. *Deep Sea Res. Part I Oceanogr. Res. Pap.* 44, 113–134. doi:10.1016/S0967-0637(96)00088-X

Seo, H., and Kim, G. (2020). Rare Earth elements in the east sea (Japan sea): Distributions, behaviors, and applications. *Geochimica Cosmochimica Acta* 286, 19–28. doi:10.1016/j.gca.2020.07.016

Shields, G., and Stille, P. (2001). Diagenetic constraints on the use of cerium anomalies as palaeoseawater redox proxies: An isotopic and REE study of Cambrian phosphorites. *Chem. Geol.* 175, 29–48. doi:10.1016/S0009-2541(00)00362-4

Sholkovitz, E. R., and Schneider, D. L. (1991). Cerium redox cycles and rare Earth elements in the Sargasso Sea. *Geochimica Cosmochimica Acta* 55, 2737–2743. doi:10.1016/0016-7037(91)90440-G

Siever, R. (1992). The silica cycle in the Precambrian. *Geochimica Cosmochimica Acta* 56, 3265–3272. doi:10.1016/0016-7037(92)90303-Z

Sillen, L. G., and Martell, A. E. (1964). *Standard constans of metal-ion complexes*. Washington, D.C: Chemical Society.

Tachikawa, K., Jeandel, C., Vangriesheim, A., and Dupré, B. (1999). Distribution of rare Earth elements and neodymium isotopes in suspended particles of the tropical Atlantic Ocean (EUMELI site). *Deep Sea Res. Part I Oceanogr. Res. Pap.* 46, 733–755. doi:10.1016/S0967-0637(98)00089-2

Takahashi, Y., Manceau, A., Geoffroy, N., Marcus, M. A., and Usui, A. (2007). Chemical and structural control of the partitioning of Co, Ce, and Pb in marine ferromanganese oxides. *Geochimica Cosmochimica Acta* 71, 984–1008. doi:10.1016/j.gca.2006.11.016

Tanaka, K., Tani, Y., Takahashi, Y., Tanimizu, M., Suzuki, Y., Kozai, N., et al. (2010). A specific Ce oxidation process during sorption of rare Earth elements on biogenic Mn oxide produced by Acremonium sp. strain KR21-2. *Geochimica Cosmochimica Acta* 74, 5463–5477. doi:10.1016/j.gca.2010.07.010

Tostevin, R., Wood, R. A., Shields, G. A., Poulton, S. W., Guilbaud, R., Bowyer, F., et al. (2016b). Low-oxygen waters limited habitable space for early animals. *Nat. Commun.* 7, 12818. doi:10.1038/ncomms12818

Tostevin, Rosalie, Shields, G. A., Tarbuck, G. M., He, T., Clarkson, M. O., and Wood, R. A. (2016a). Effective use of cerium anomalies as a redox proxy in carbonate-dominated marine settings. *Chem. Geol.* 438, 146–162. doi:10.1016/j.chemgeo.2016.06.027

Voigt, M., Mavromatis, V., and Oelkers, E. H. (2017). The experimental determination of REE partition coefficients in the water-calcite system. *Chem. Geol.* 462, 30–43. doi:10.1016/j.chemgeo.2017.04.024

Wallace, M. W., Hood, A., Shuster, A., Greig, A., Planavsky, N. J., and Reed, C. P. (2017). Oxygenation history of the Neoproterozoic to early Phanerozoic and the rise of land plants. *Earth Planet. Sci. Lett.* 466, 12–19. doi:10.1016/j.epsl.2017.02.046

Wang, R., Williams, T. J., Hillenbrand, C. D., Ehrmann, W., Larkin, C. S., Hutchings, A. M., et al. (2022). Boundary processes and neodymium cycling along the Pacific margin of West Antarctica. *Geochimica Cosmochimica Acta* 327, 1–20. doi:10.1016/j.gca.2022.04.012

Webb, G. E., and Kamber, B. S. (2000). Rare Earth elements in holocene reefal microbialites: A new shallow seawater proxy. *Geochimica Cosmochimica Acta* 64, 1557–1565. doi:10.1016/S0016-7037(99)00400-7

Yaitskaya, N. (2011). *Temperature, salinity, oxygen, phosphate, silicate, nitrite, pH and alkalinity data collected in the Black sea, tyrrhenian sea and western basin from R/vs GORIZONT and OKEANOGRAF, 1960 - 1969 (NCEI accession 0074609).Alkalinity and pH used*. Russia: NOAA National. Russian Academy of Science.

Zhang, J., and Nozaki, Y. (1998). Behavior of rare Earth elements in seawater at the Ocean margin: A study along the slopes of the sagami and nankai troughs near Japan. *Geochimica Cosmochimica Acta* 62, 1307–1317. doi:10.1016/S0016-7037(98)00073-8

Zhang, J., and Nozaki, Y. (1996). Rare Earth elements and yttrium in seawater: ICP-MS determinations in the east caroline, coral sea, and South Fiji basins of the Western South Pacific ocean. *Geochimica Cosmochimica Acta* 60, 4631–4644. doi:10.1016/S0016-7037(96)00276-1

Zhang, K., and Shields, G. A. (2022). Sedimentary Ce anomalies: Secular change and implications for paleoenvironmental evolution. *Earth-Science Rev.* 229, 104015. doi:10.1016/j.earscirev.2022.104015

Zhang, L., Chan, L. H., and Gieskes, J. M. (1998). Lithium isotope geochemistry of pore waters from ocean drilling program sites 918 and 919, irminger basin. *Geochimica Cosmochimica Acta* 62, 2437–2450. doi:10.1016/S0016-7037(98)00178-1

Zheng, X. Y., Plancherel, Y., Saito, M. A., Scott, P. M., and Henderson, G. M. (2016). Rare Earth elements (REEs) in the tropical South Atlantic and quantitative deconvolution of their non-conservative behavior. *Geochimica Cosmochimica Acta* 177, 217–237. doi:10.1016/j.gca.2016.01.018